Ninth International Conference on
THIN-WALLED STRUCTURES – ICTWS2023
Sydney, Australia, Nov 29 – Dec 1, 2023

EXPERIMENTAL STUDY ON THE FATIGUE PERFORMANCE AND DAMAGE EVALUATION OF V125 STEEL ROOFING CLADDING UNDER TYPHOON HAZARDS

Fan Bai[1,2], Na Yang[1,2], Hanwen Ge[1,2], Yunxin Li[1,2]

1. School of Civil Engineering, Beijing Jiaotong University, No.3 Shangyuancun, Beijing,100044, China

2. Beijing's Key Laboratory of Structural Wind Engineering and Urban Wind Environment,

3. Shangyuancun, Beijing, 100044, China

Keywords: Steel roof cladding, fatigue damage, damage evaluation, design typhoon.

Abstract: *This paper presents a research related fatigue properties of a V125 type steel roofing cladding and its probabilistic evaluation under typhoon hazards. The fatigue performance of this typical screw-fastened steel roof cladding is studied with cyclic load test. The fatigue process in the crack nucleation and propagation stages as well as the final failure modes are obtained. The number of cycles of applied load at crack failure (N_f) are recorded. The generalized S-N curve for the fatigue failure of the roof sheeting was then curve-fitted from the experimental data. The fatigue damage evaluation of the cladding under a "design typhoon" was later presented, which provide a fatigue resistance degradation model for the steel roof cladding. The results of this study may contribute to the assessment of the fatigue performance of light steel roof cladding under typhoon hazards.*

Highlights:

1. Present the fatigue performances and failure modes of the V125 steel roof cladding.
2. Classify the generalized S-N curves of V125 steel roof cladding.
3. Conduct damage evaluation of V125 steel roof cladding under a design typhoon.

1 INTRODUCTION

Trapezoidal corrugated steel roof cladding made of thin-walled grade Q235, Q345 and G550 steel are widely used in industrial buildings in China. Fig.1a shows a V125 type steel sheeting commonly found in industrial or residential buildings, and Fig.1b shows the associated ST5.5 type fixing screw, these two components concluded the V125 type steel roofing cladding.

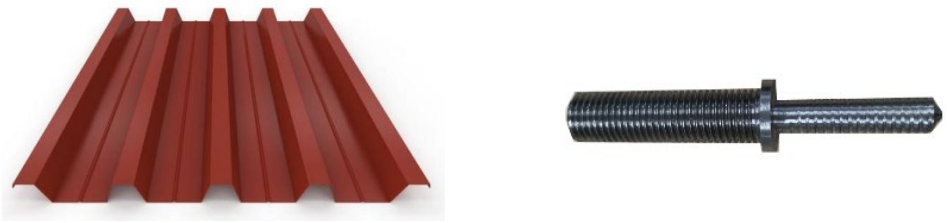

a. V125 type sheeting b. ST5.5 type screw

Figure 1: V125 type steel roofing cladding.

These steel roof cladding may suffer static and fatigue damages during strong wind such as the hurricane or typhoon in their service life. In the past few decades, some studies have

documented the severe damages of steel roof cladding during the passage of tropical typhoon (Morgan and Beck, 1977, Beck and Stevens, 1979, Pan et al., 2005, Yang et al., 2018). It was clearly observed that the sheeting failed in the proximity of the roof fasteners due to sustained fluctuating uplift wind load.

The damage of sheeting around the roof fasteners can generally be classified into static and fatigue failures. Research on the first group of failures includes Xu and Teng (1994) and Lovisa et al. (2016) who applied different finite element models to investigate the local plastic behavior of trapezoidal sheeting under monotonic loads. Mahendran (1994) adopted different experimental approaches to clarify the effects of various structural parameters on the static performance of the roofing systems with different scales and spans, including the plate thickness, yield limit and screw size. Additionally, different local failure modes of the roofing systems under wind suction were summarized.

The fatigue failures are more striking than the static failures since they may occur at a lower load level than the static capacity. Morgan and Beck (1977) and Beck and Stevens (1979) conducted a series of experiments to investigate the possibility of wind-induced fatigue damage of screw-fastened roofing systems. They concluded that fatigue damage near the fasteners may lead to the failure of the steel roof cladding during typhoon Tracy. Lynn and Stathopoulus (1985) also highlighted the importance of wind-induced fatigue damage to metallic buildings. Mahendran (1994) carried out experimental investigations to examine the fatigue performance of different roofing systems under different cyclic loads. Extensive studies were also conducted on appropriate testing methods on the fatigue failure problem during a typhoon. The Darwin Area Building Manual (1976), the Guidelines for the testing and evaluation of products for typhoon prone areas (Technical Record 440 1979) was published immediately after the passage of typhoon Tracy as references for any roofing system that requires proof test on its fatigue resistance. Further studies found that the TR440 test was conservative for trapezoidal cladding but not conservative for corrugated cladding (Xu 1996, Mahendran 1994). The UK Building Research Establishment developed a load cycle calculation method by counting the peak loads obtained from 20 most severe storms in the 50-year return period. Kumar (2000) proposed a load simulation methodology in the fatigue study of the roof cladding, which thoroughly consider the Gaussian and non-Gaussian wind pressure fluctuations. And, it should be noted that the fatigue life of roof cladding would be overestimated due to the overlooked non-Gaussian properties of fatigue loads. Xu (1996) systematically assessed the fatigue load and damage of wind-induced roof system using experimental and theoretical methods. The S-N curves of different roofing systems and the fatigue damage factor were presented based on the modified Miner criterion.

Mahendran (1989) and Henderson (2010, 2011) also identified the categories of crack formation and the locations of most severe crack. They also categorized the various crack formations into two groups, i.e. the crease crack group and the star crack group. The crease crack group consists of any cracks that initiated away from the fastener in regions of plastic deformation. It consists mainly the ‘H’ cracks, known as Type A crack and the ‘T’ cracks. The star crack group comprises cracks initiated at the hole edge.

Mahendran (1994) have also conducted small isolated cladding-fastener tests to investigate the static pull-through failure of cladding. They successfully extended the small-scale test to study the fatigue response of roof cladding. Both the static and fatigue failure problems may then be narrowed down to the failure of a small area around one critical fastener rather than failure in the whole cladding sheet. This method can provide dimpling and plastic deformation surrounding the fastener for static failures. The small-scale test arrangement yielded similar fatigue strength to that from full scale roof cladding tests in the fatigue studies. However, no information was reported on the type of crack formations using the small-scale arrangement.

To the best knowledge of the authors, most of the existing researches primarily focused on the fatigue damage phenomena of high-strength steel cladding. Nevertheless, the effects of fatigue failures on low-yield strength steel cladding have not been clearly elucidated. There is also a lack of experience in using the small-scale test arrangement to investigate the fatigue damage evolution of the steel roof claddings. Hence, this paper aims to address the above mentioned issues and further improve the understanding of fatigue performance of screw-fastened steel roof cladding under strong typhoons. The fatigue performance of a common type of profiled roofing sheets, V125 type steel roof cladding, was studied via small-scale test arrangement. Three static tests were carried out to determine the static pull-through capacity (*SPC*) followed by tests on 24 specimens with different constant amplitude cyclic loadings. The failure modes and evolution of damage were classified with information on the fatigue development. The generalized S-N curve for fatigue failure of the roof sheeting was curve-fitted from experimental data. A fatigue damage evaluation under a designed typhoon was then proposed, which provide the fatigue resistance degradation model for the steel roof cladding.

2 Experimental Methodology

2.1 Specimens and arrangements

A total of 27 steel roof claddings made of V125 type roofing sheet and ST5.5 type screws were test in the laboratory. All specimens are grade Q235 steel with 235 MPa nominal yield stress and 1.96×10^5 MPa Young's modulus. The dimensions of the sheeting and screw are shown in Fig.2. The ST5.5 type screw is at the center of the array of M8 screws as shown in Fig.2(c). The test specimens were connected to 340×320×20mm steel plate below as shown. The latter serves as foundation to transfer the load.

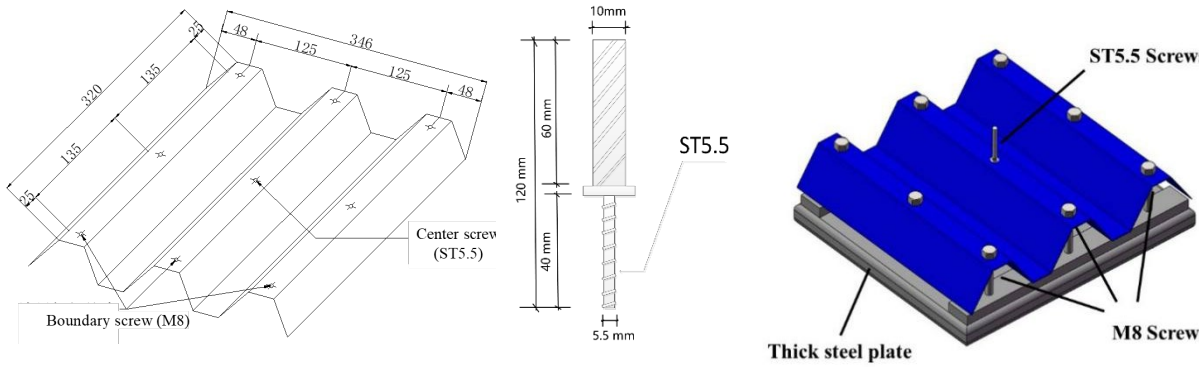

(a) V125 type sheeting (unit: mm) (b) ST 5.5 Screw (c) thick steel plate at other eight nodes

Figure 2: Roof sheets and fasteners in test.

As shown in Fig.3, a small-scale test arrangement was designed for this investigation. An actuator vertical load was applied to the bottom of the thick steel plate. The displacement transducer was connected in the top of the ST5.5 screw. The upward movement of the thick steel plate was driven by the actuator to simulate the actual wind action, until the steel roof cladding is broken.

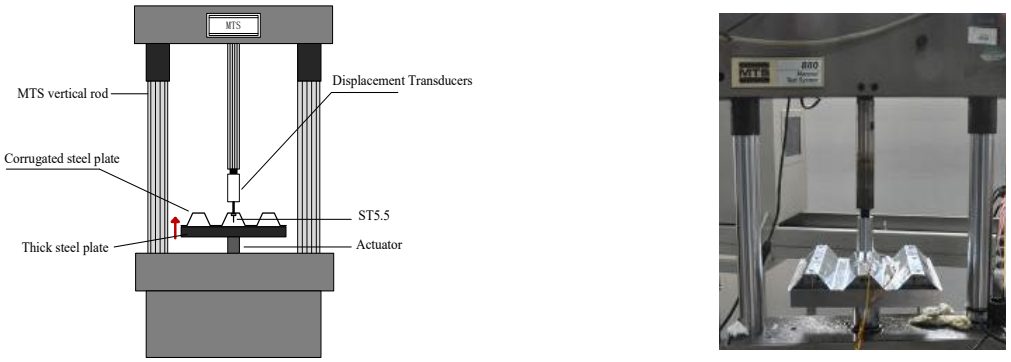

Fig.3: Small-scale test specimens and arrangements

2.2 Test method

Three static tests were conducted to determine the static pull-through capacity (*SPC*) of the steel roof claddings. The *SPC* can be used to determine the upper bound of the *S-N* curve of the roof cladding. Twenty-four tests under constant cyclic load were then carried out to determine the fatigue life and thereby produce the *S-N* curve. The load amplitude was determined as percentages (20%-90%) of the measured *SPC* of the cladding as shown in Table 1. The load cycle number at crack failure (N_f) in the steel roof cladding was also recorded. Table 1 shows the test load amplitude for each test series. *T* denotes the static test series, and *F* denotes the fatigue test series. Max. Cyclic Load denotes the maximum value of the cyclic load while Min. Cyclic load denotes 10% of the Max. Cyclic load. There are three test specimens at each load level. Table 2 shows the elastic modulus, yield strength, ultimate tensile strength and the ratio of the ultimate tensile strength to the yield strength of the steel roof cladding obtained from material tests.

Table 1: Test load information

Test Number	Min/Max. Cyclic Load (% *SPC*)	Min/Max. Cyclic Load (N)	Test Number	Min/Max. Cyclic Load (% *SPC*)	Min/Max. Cyclic Load (N)
T-1	-	1552	F5	-50%	-78.5/-785
T-2	-	1568	F6	-60%	-95/-950
T-3	-	1571	F7	-70%	-109.6/-1096
F2	-20%	-31.3/-313	F8	-80%	-125/-1250
F3	-30%	-95/-950	F9	-90%	-141/-1410
F4	-40%	-62.6/-626	-	-	-

Table 2: Material test results for the steel roof claddings

Test number	Elastic Modulus (MPa)	Yield Strength (MPa)	Ultimate tensile strength (MPa)	Ultimate tensile strength / Yield Strength
1	196682	364	396	1.09
2	190638	352	390	1.11
3	200754	375	397	1.06
Mean	196024	364	394	1.08

3 TEST RESULTS AND DISCUSSIONS

3.1 Failure Mode

The failure modes of the steel roof cladding at different cyclic load levels are shown in Fig. 4. They can be categorized into two groups with respect to the load amplitude: one group consists of the pull out failure (*PO*) with a loading range of 20% to 50% of *SPC*. The other group consists of the pull-through failure (*PT*) with a loading range of 50% to 90% of *SPC*. The shape of cracks in the *PO* failure mode has a 'Star' shape transversely and longitudinally, and that of the *PT* failure mode is in the form of an '*I*' shape transversely. The demarcation point of the two types of failure modes is 50% *SPC*, when both types of failure modes may appear at this cyclic load level (Figs. 4e, 4f). When the cyclic load amplitude was less than 50% *SPC*, cracks were generated both longitudinally and transversely around the nodal holes, leading to cracking of the plates around the holes. There was no obvious plastic deformation in the roof cladding (Figs. 4h, 4i, 4j) at this low load amplitude. The area around the screw fastener hole suffered from obvious plastic deformations when the cyclic loading amplitude is greater than 50% *SPC*. Large-cyclic loading could induce plastic deformation in the middle of the steel roof cladding.

a）90% *SPC* b）80% *SPC* c）70% *SPC* d）60% *SPC* e）50% *SPC*

f）50% *SPC* g）40% *SPC* h）40% *SPC* i）30% *SPC* j）20% *SPC*

Fig.4: Fatigue failure modes patterns

3.2 Fatigue damage process and mechanism analysis

The failure process of the steel roof cladding composes of crack initiation and its development under constant cyclic load. Cracks in the cladding can be found around the screw fastener in each failed specimen. The fatigue test specimen are noted to experience the

following two stages in the fatigue evolution process: i.e., a steady rate increment period in the crack nucleation stage, and a rapid increment period in the crack propagation stage.

The behavior of one specimen in *F*4 test series is discussed in details as an example to describe the *PO* failure shown in Fig.5:

(1) Crack nucleation stage (0-32800 numbers of loading cycles): There was no obvious plastic deformation observed around the fastener in this stage. The condition of the steel roof cladding was stable (see Fig. 5a).

(2) Crack propagation stage (32800-64529 numbers): The crack zone caused by the presence of micro cracks around the screw holes increased slowly. The steel cladding roof around the hole completely separated from the screw with no obvious plastic deformation in the cladding (see Fig. 5b and Fig.5c).

a. The crack nucleation stage

b. The crack propagation stage

c. Roof sheeting breaks apart with crack

Fig.5: Failure process of F4 test

The behavior of one specimen in F7 test series is described below to illustrate the development of the *PT* fatigue failure shown in Fig.6:

(1) Crack nucleation stage (0-7400 numbers): Significant plastic deformation was found in the cladding at the end of the first loading cycle. The steel plate around the screw was in a stable plastic stage.

(2) Crack growth stage (7400-8211 numbers): Deformation of the cladding around the hole increased significantly with visible cracks at the edge of the up flange (see Fig. 6b). After the screw was separated from the cladding, obvious cracks on both side of the hole can be observed in the transverse direction of the cladding. (see Fig. 6c).

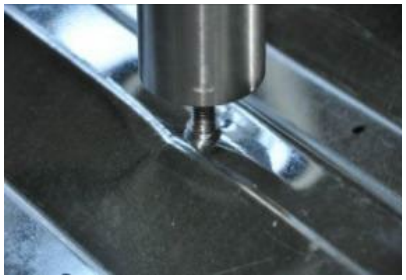

a. The crack nucleation stage

b. The crack propagation stage.

c. Roof sheeting breaks apart with crack

Fig.6: Failure process of *F7* test specimen

Table 3 shows the number of loading cycles at crack failure (N_f) in different crack propagation stages. N_f was found decreasing with the maximum cyclic load amplitude.

Table 3: Fatigue test results of V125 steel roof cladding

Sample No.	Max. cyclic load (% of *SPC*)	Number of Cycles to failure (N_f)	Sample No.	Max. cyclic load (% of *SPC*)	Number of Cycles to failure (N_f)
*F*2-1	20	350121	*F*2-2	20	228047
*F*2-3	20	351757	*F*3-1	30	51041
*F*3-2	30	33866	*F*3-3	30	69301
*F*4-1	40	64529	*F*4-2	40	66023
*F*4-3	40	43926	*F*5-1	50	33513
*F*5-2	50	42092	*F*5-3	50	22739
*F*6-1	60	26349	*F*6-2	60	11497
*F*6-3	60	15486	*F*7-1	70	8798
*F*7-2	70	11361	*F*7-3	70	8221
*F*8-1	80	4444	*F*8-2	80	5063
*F*8-3	80	5619	*F*9-1	90	3430
*F*9-2	90	1605	*F*9-3	90	1378

3.3 Fatigue life

As shown in Table 3, the fatigue life of the V125 steel roof cladding is presented, then the S-lgN_f curve can be curve-fitted from the results in semi-logarithmic scale in Fig.7with the following regression:

$$S=3330-564.84\lg N_f \quad (1)$$

where S represents the applied load at the steel roof cladding. N_f denotes the fatigue life of the roof cladding.

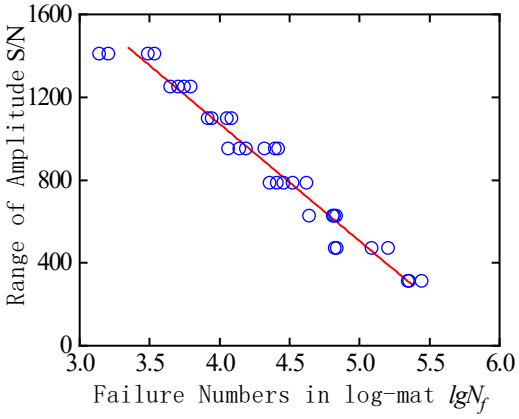

Fig.7: Fatigue life curve of the V125 steel roof cladding

4 FATIGUE DAMAGE EVALUATION OF THE V125 STEEL ROOF CLADDING UNDER ONE TYPHOON

The fatigue damage evaluation of the roof cladding induced by a “design typhoon” consists of three steps. Firstly, the specification of “design typhoon” was presented. Secondly, estimating of wind load cycles accounting for the wind speed and wind directions. Finally, the damaged evaluation of steel roof cladding caused by a tropical typhoon was developed.

4.1 Specification of "design typhoon"

A structure on ground will experience a general change in wind speed and direction during the passage of a typhoon. On the passage of the typhoon, the worst winds are normally experienced by structures located adjacent to the path of the edge of the eye. As shown in Fig.8, this paper provided a similar 'design typhoon' which was original developed by (Jancauskas 1994) specifically for fatigue related applications. The design typhoon are specified in combination of the wind speed and direction, its duration was assumed to be 300 minutes (five hours). The analysis interval was then set as 15min, except for the 1st and 21st time interval for which it was 7.5min, then there will be 21 analysis interval concluded the duration. The mean wind speed and direction were assumed constant during each analysis interval. The typhoon is characterised by a structure of circulating wind surrounding a calm eye, R denotes the radius of the vortex, r means the distance between the center of the calm eye and the buildings. Based on observational data from past typhoons (Walker 1988), an empirical formulas was proposed for calculating the maximum wind speed from the typhoon center, as shown in Eq.(2). As the 6th interval shown in Fig.8, the wind speed, v, at a particular location in the buildings during a tropical typhoon included two terms added in vector, the tangential velocity $V_P(R/r)^k$ and forward velocity KU. V_P is a function of the central pressure, K is the terrain friction loss factor, U means the forward speed of the eye. Thereafter, the test house at the 11th time interval will be at the 2.5 hours when the radius of the vortex R equal to the distance between the center of the calm eye and the buildings r.

$$v = V_P(R/r)^k + KU \tag{2}$$

where $V_p^{`} = C\sqrt{1010 - p}$, the gust factor is 1.7, p equals to 930mb, U equals to 4.17m/s, R equals to 25 km, C and k can be fitted by typhoon data (Walker, Reardon 1988), p is center atmospheric pressure of typhoon. K equals to 0.5, C equals to 4.5, k is a constant which equals to 0.67.

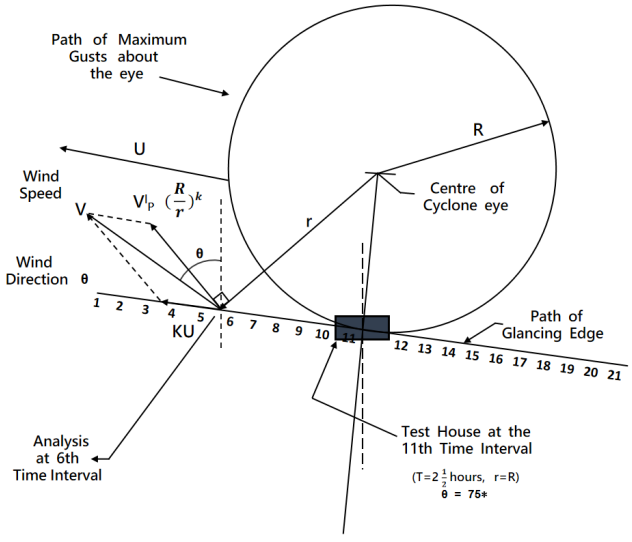

Fig.8 The details of wind speed and direction in the design typhoon

4.2 Determination of the fatigue wind loading matrix

The wind load for a screw placed in the roof system can be obtained from the Eq.(3), where ρ denotes the air density, C_P denotes the wind pressure coefficient, v denotes the wind speed, and A represents the tributary area for the screw.

$$S_i = \frac{1}{2}\rho C_P v^2 A \tag{3}$$

The time history data of the wind pressure coefficient C_P is taken from the Aerodynamics Database of Tokyo Polytechnic University (TPU 2007) where the cyclic range come from the wind pressure coefficient fluctuations. The database is obtained based on wind tunnel tests of low-rise buildings, where the model scale ratio is 1/100, the speed scale ratio is 1/3 and the time scale ratio is 3/100. Each series data of 15° contains 9000 time-varying wind pressure coefficients, the wind tunnel acquisition frequency is 15Hz with an acquisition time of 600s. The wind tunnel test conditions simulate the topographical conditions of the suburbs, in which the length, width and height of the house model are 160:240:4, the actual dimension of the building are 240mm, 160mm and 40mm for the length, width and height, respectively. As shown in Fig.9a, the red pressure point at the corner of the roof is taken as the research object. The tributary wind area of each screw is assumed to be 0.25 square meters.

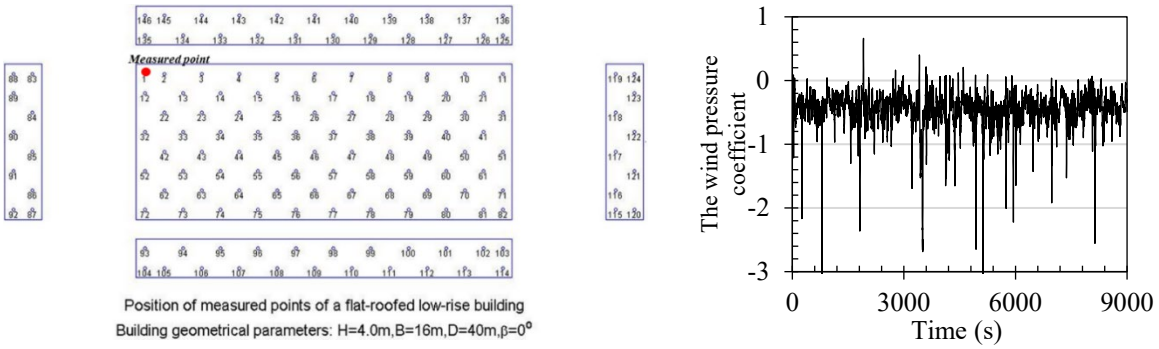

a. Position of measured points b. Wind pressure coefficient time history

Fig.9: Information of wind pressure coefficient

The rain-flow method in reference (Jancauskas et,al. 1994) can identify cycles as closed hysteresis loops and provide range and mean values for each cycle. Common cycle counting techniques in use today are peak, range, range-pair and rain-flow. Of these various methods, rain-flow method has been shown to be superior and yields the best fatigue life estimates, especially in the case of broadband non-Gaussian process . The rain-flow method can identify cycles as closed hysteresis loops and can provide range and mean values for each cycle. This method was used by Xu (1995) and Jancauskas et,al. (1994) to count the cycles of wind-induced pressures. Therefore, this method has been adopted in this study to count the number of cycles present in pressure fluctuations.

Totally, 7 full scale wind pressure coefficient (from 30 degree to 120 degree in 15 degree interval) matrix were mentioned above. As shown in Table 4, the wind pressure coefficient matrix at 45° is presented as a representative example. Based on the wind load fatigue characteristics, the damage value at different time intervals can be calculated by Minner damage criterion (Xu 1991).

Table 4: Wind pressure coefficient matrix at 45°

Range / Mean	0.2	0.6	1.0	1.4	1.8	2.2	2.5	2.9	3.3	3.7
0.1	92	1.5	0	0	0	0	0	0	0	0
0.4	590.5	48.5	5	2	0	0	0	0	0	0
0.6	291	32	13	6	2	1	0	0	0	0
0.9	28	3	1	1	2	1	0	0	0	0
1.2	8	2	0	0	0	2	2	0	0	0
1.4	2	1	0	0	0	0	1	1	0.5	0
1.7	0	0	0	0	0	0	0	0	0.5	0
2.0	1	0	0	0	0	0	0	0	0	1
2.2	1	0	0	0	0	0	0	0	0	0
2.5	2	0	0	0	0	0	0	0	0	0

The results of wind pressure coefficient matrix at 45° calculated by the rain-flow method in terms of the maximum pressure cycle range , the number of load cycles in model scale are listed in Table 4. Based on wind tunnel data, a full-scale fatigue wind load matrix was obtained in each time interval by employing Eq.(4) (Jancauskas 1994).

$$N_f = N_{wt} \cdot \frac{v}{V_{wt}} \cdot \frac{T_1}{T_{wt}} \cdot \frac{1}{S_r} \tag{4}$$

where N_f denotes the cycle number of full-size fatigue wind load matrix, N_{wt} denotes the number of loops, which means the maximum wind pressure minus the minimum wind pressure, v denotes the wind speed in Fig.8, T_1 is the duration of the speed v, V_{wt} means the wind speed in the wind tunnel, T_{wt} denotes the time for the wind tunnel test, the model scale ratio S_r is 1/100. Then, the 45° full scale wind pressure coefficient matrix at the wind speed v of 36 m/s is taken as an example, as shown in Table 5. The full scale wind pressure coefficient matrix for the other degrees can be referred to the reference (Ge, 2019).

Table 5: 45° full scale wind pressure coefficient matrix

Range / Mean	0.2	0.6	1.0	1.4	1.8	2.2	2.5	2.9	3.3	3.7
0.1	697	11	0	0	0	0	0	0	0	0
0.4	4475	368	38	15	0	0	0	0	0	0
0.6	2205	243	99	45	15	8	0	0	0	0
0.9	212	23	8	8	15	8	0	0	0	0
1.2	61	15	0	0	0	15	15	0	0	8
1.4	15	8	0	0	0	0	8	8	4	0
1.7	0	0	0	0	0	0	0	0	4	0
2.0	8	0	0	0	0	0	0	0	0	0
2.2	8	0	0	0	0	0	0	0	0	0
2.5	15	0	0	0	0	0	0	0	0	0

4.3 Fatigue damage evaluation

The fatigue characteristic curve (S-N curve) of the steel roof cladding is taken from Eq.(1) which is fitted from the constant amplitude fatigue test (Table 3). Thereafter, the fatigue damage of the steel roof cladding was calculated based on Eq.(5) through the Miner's rule (Xu 1991). Wind-induced fatigue damage, *D*, can be estimated using the well-known damage accumulation hypothesis of Miner's rule:

$$D = \sum_{i=1}^{k} \frac{n_i}{N_i} \tag{5}$$

where, n_i= total number of wind load cycles in the *i*th block of constant pressure range; N_i= number of cycles to failure; and k= total number of blocks.

As shown in Table 6, the damage value represents the cumulative damage created during each time interval. The distribution curve of the cumulative damage value (maximum wind speed, v=36m/s) with the action time of the typhoon is obtained.

Table 6: Typhoon-induced damage distribution from one design cyclone (v=36m/s)

The typhoon duration (minute)	Wind ection egree)	Wind speed (m/s)	Accumulated damage	The typhoon duration (minute)	Wind ection egree)	Wind speed (m/s)	Accumulated damage
7.5	41	31	0.007	172.5	79	36	0.022
22.5	44	32	0.014	187.5	83	36	0.020
37.5	46	33	0.014	202.5	87	36	0.018
52.5	49	34	0.016	217.5	90	35	0.016
67.5	53	34	0.016	232.5	94	35	0.016
82.5	56	35	0.017	247.5	97	34	0.016
97.5	60	35	0.018	262.5	101	34	0.016
112.5	63	36	0.019	277.5	104	33	0.016
127.5	67	36	0.021	292.5	106	32	0.015
142.5	71	36	0.023	300.0	109	31	0.007
157.5	75	36	0.024	-	-	-	-
Total damage value			-	-	-	-	0.349

Fig.11 shows the accumulation of fatigue damage over time at different extreme wind speeds over a 15-minute analysis interval. It can be seen from Fig.10, the damage value will increased as the time and the maximum wind speed increased.

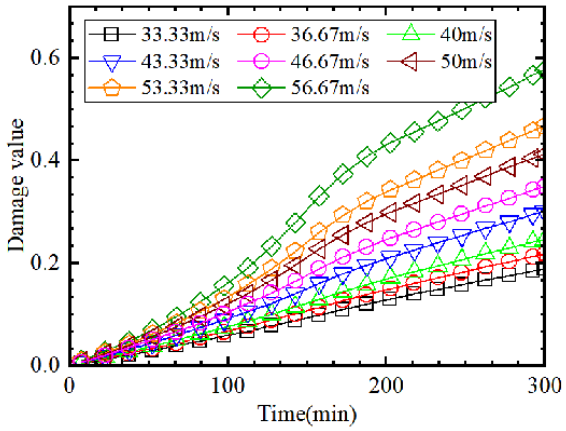

Fig.10: Typhoon-induced damage accumulation curve

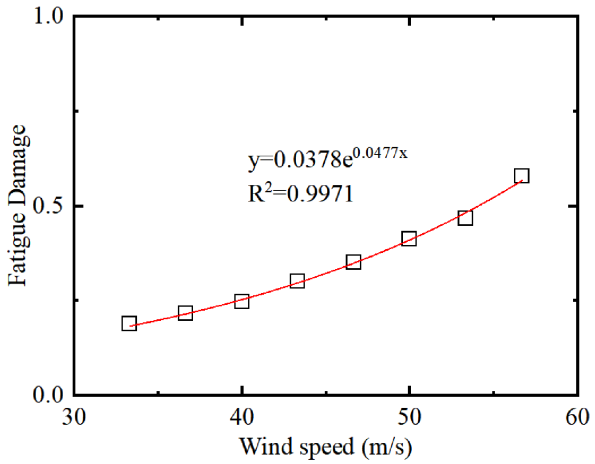

Fig.11 The wind-induced fatigue damage curve for the steel roof cladding versus wind speed

$$D \tag{6}$$

Fig.11 shows the wind-induced fatigue damage curve for the steel roof cladding versus wind speed. The wind-induced fatigue damage D of the V125 steel roofing cladding curve versus wind speed v was fitted as a experiential function shown in Eq.(6). Table7 show the comparison of the fatigue damage estimation between the V125-type steel roof cladding and another typical steel roof cladding widely used in Australia, No. 14×50mm Type 17 self-drilling screws with the corrugated steel roof cladding (0.42mm base metal thickness and a minimum material yield strength of 550 MPa), as shown in reference (Jancauskas 1994). The results show that these two types of steel roof cladding have the same trend. It can be also found that the fatigue damage of steel cladding roofs with low yield strength were lower than that of high yield strength in the peak wind speed of 46.7m/s and 50m/s, while it seems in a similar status at the peak wind speed of 43.4m/s. However, the fatigue damage of low yield strength was larger than that in high yield strength steel at the wind speed of 40.0m/s. It seems that the fatigue damage of the high yield strength steel was more sensitive in the high peak wind speed while fatigue damage of the low yield strength steel was sensitive in low peak wind speed.

Table 7: Comparison of accumulated damage after 5 hours

wind speed	Accumulated fatigue damage after 5 hours	Accumulated fatigue damage after 5 hours (Jancauskas et,al. 1994)
50.0 m/s	0.413	1.440
46.7 m/s	0.350	0.742
43.4m/s	0.301	0.321
40.0 m/s	0.246	0.109

5 CONCLUSIONS

In this paper, the fatigue performance and damage evaluation of V125-type steel roof cladding was presented based on experimental method. The different stages of fatigue failure were summarized and the general *S-N* equations for the typical steel roof cladding was also provided. Based on the obtained results, the fatigue damage after the design typhoon was presented with respect to the different wind speed values. A experiential function was fitted to describe the damage evolution of wind-induced fatigue of the steel roof cladding under various typhoons. The fatigue damage of the high yield strength steel was more sensitive in the high peak wind speed while fatigue damage of the low yield strength steel was sensitive in low peak wind speed.

Acknowledgements

The comments and help from Prof. S.S. Law in polishing the English usage of this paper are gratefully acknowledged. The study presented in this paper was supported by the Fundamental Research Funds for the Central Universities (2022XKRC006), National Natural Science Foundation of China (52008020), and 111 Project of China (B13002).

REFERENCES

[1] Morgan, J., Beck, V. Failure of Sheet-metal Roofing under Repeated Wind Loading.pdf. *Civ. Eng. Trans*, 1977. **138**: p. 290-294.

[2] Beck, V., Stevens, L. Wind loading failures of corrugated roof cladding. *Civ. Eng. Trans*, 1979. **19**: p. 1-5.

[3] Pan, S., Shi, Y., Geng, X., Lu, S. Cause Analysis of Damages to Industrial Workshops in Taizhou of Zhejiang by typhoon 0401 and Exploration of Countermeasures. *Steel Structures*, 2005. **20**(6): p. 52-57.

[4] Yang, Q., Gao, R., Bai, F., Li, T., Tamura, Y. Damage to buildings and structures due to recent devastating wind hazards in East Asia. *Natural Hazards*, 2018. **1**(1): p. 1-33.

[5] Xu, Y.L., Teng, J.G. Local plastic failure of light gauge steel roofing sheets - finite element analysis versus experiment. *Journal of Constructional Steel Research*, 1994. **30**(2): p. 125-150.

[6] Lovisa, A.C., Henderson, D.J., Ginger, J.D., Walker, G. Characterising fatigue macrocrack initiation in profiled steel roof cladding. *Engineering Structures*, 2016. **125**: p. 364-373.

[7] Mahendran, M. Behaviour and design of crest-fixed profiled steel roof claddings under uplift wind. *Engineering Structures*, 1994. **16**(5): p. 368-376.

[8] Lynn, B.A., T.Stathopoulos. Wind-induced Fatigue on Low Metal Buildings. *Journal of Structural Engineering*, 1985. **111**(4): p. 826-839.

[9] Xu, Y.L. Wind-induced fatigue loading and damage to hip and gable roof claddings. *Journal of Structural Engineering*, 1996. **122**(2): p. 1475-1483.

[10] Mahendran, M. Effect of Overload Cycles on Thin Steel Roof Claddings during Cyclonic Winds. *Journal of Testing and Evaluation*, 1994.

[11] Kumar, K.S. Prediction of wind-induced fatigue on claddings of low buildings. *Computers and Structures*, 2000. **75**: p. 31-44.

[12] Mahendran, M. Fatigue behavior of corrugated roofing under cyclic wind loading. 1989, James Cook typhoon Structural Testing Station.

[13] Henderson, D.J. Response of pierced fixed metal roof cladding to fluctuating wind loads. 2010, James Cook University.

[14] Henderson, D.J., Ginger, J.D. Response of pierced fixed corrugated steel roofing systems subjected to wind loads. *Engineering Structures*, 2011. **33**(12): p. 3290-3298.

[15] Boughton, G.N., Henderson, D.J., Ginger, J.D., , J.D.H., Walker, G.R., Leitch, C.J., Somerville, L.R., Frye, U., Jayasinghe, N.C., Kim, P.Y. Tropical typhoon Yasi Structural damage to buildings. 2011, School of Engineering and Physical Sciences, James Cook University.

[16] Jancauskas, E., Mahendran, M., Walker, G. Computer simulation of the fatigue behavior of roof cladding during the passage of a tropical typhoon. *Journal of Wind Engineering and Industrial Aerodynamics*, 1994. **51**: p. 215-227.

[17] Walker, G.R., Reardon, G.F., Jancauskas, E.D. Observed effects of topography on the wind field of typhoon winifred. *Journal of Wind Engineering & Industrial Aerodynamics*, 1988. **28**(1): p. 79-88.

[18] Aerodynamic database for low-rise buildings. 2007, Tokyo Polytechnic University: Tokyo.

[19] Xu, Y.L. Fatigue performance of screw-fastened light-gauge-steel roofing sheets. *Journal of Structural Engineering*, 1995. **121**(3): p. 389-398.

[20] Xu, Y.L. Fatigue damage estimation of metal roof cladding subject to wind loading. *Journal of Wind Engineering and Industrial Aerodynamics*, 1997. **72**: p. 379-388.

[21] Ge, H.W. Fatigue calculation model of screw joints used in light-weight steel roof and its application in post-disaster assessment. 2019, Beijing Jiaotong University (in Chinese).

[22] DABM, Darwin area building manual, Darwin Reconstruction Commission, the Northern Territory of Australia, 1976.

[23] TR440, Guidelines for the testing and evaluation of products for typhoon prone areas. Tech. Record 440. Experimental Building Station. Dept. of Housing and Construction, Australia, 1978.